

# A Unified Constitutive Equation of a Bainite Steel During Hot Deformation

Lixin Li, Ben Ye, Sheng Liu, Shengde Hu, and Hanqing Liao

(Submitted November 29, 2015; in revised form August 7, 2016; published online August 25, 2016)

A constitutive model has been established based on dislocation theory, work hardening and dynamic recovery theory, and softening mechanisms of dynamic recrystallization. The stress-strain curves of a bainite steel have been measured with hot compression experiments at temperatures of 1173, 1273, 1373 and 1473 K with strain rates of 0.01, 0.1, 1 and 10 s<sup>-1</sup> on a thermo-mechanical simulator (Gleeble-1500). The material constants involved in the constitutive model have been optimized by an inverse analysis of the stress-strain curves using the method of coordinate rotation, determining the strain-stress relationship or the constitutive equation, the kinetic models of dynamic recovery and dynamic recrystallization, and a few material constants of the investigated steel. Comparison of the calculated flow stress with the experimental data suggests that the relationship between the flow stress and the strain rate, temperature, strain of the steel during hot deformation can be described by the constitutive model, and that the underlying materials science can be captured from the material constants determined by the stress-strain curves.

**Keywords** bainite steel, constitutive equation, compression test, hot deformation, recrystallization

## 1. Introduction

Numerical simulation technology has been widely applied to the study of metal deformation process in recent years. An accurate constitutive equation for flow stress is the key to improving the accuracy of the numerical simulation. Therefore, it is essential to establish an accurate functional relation between flow stress and deformation parameters. A number of constitutive equations were developed to describe the hot deformation behaviors of alloys (Ref 1-5). These equations can be classified into two groups, namely empirical and physical models. Empirical models focus on phenomenological modeling of the flow stress using mathematical methods. Physical models are based on the deformation mechanisms of alloys. When the physical models have been determined, it is possible to quantitatively explore the rules of materials science during hot deformation process.

The hot deformation of alloys is followed with work hardening (WH) and dynamic recovery (DRV). When the deformation degree exceeds a critical strain for a given temperature and strain rate, dynamic recrystallization (DRX) will occur. The stress-strain relationship in the stage of WH and DRV may be expressed by dislocation model (Ref 5, 6). It is found that the Avrami equation is applicable for describing the

DRX kinetics (Ref 7, 8). Therefore, it is complete to establish the physical models to express the stress-strain relationship during high-temperature deformation of alloys once the critical strain for the onset of DRX is determined. When the strain hardening rate is expressed as  $\theta$ , or  $\theta = d\sigma/de$ , where the  $\sigma$  and  $\epsilon$  are flow stress and strain, the critical values of flow stress and strain that correspond to the initiation of DRX under arbitrary conditions of deformation can be calculated by a criterion of  $\frac{\partial}{\partial \sigma} \left( -\frac{\partial \theta}{\partial \sigma} \right) = 0$  based on the principles of irreversible thermodynamics (Ref 9). This criterion with a very clear physical meaning has been adopted by many literatures (Ref 10, 11). It also shows that the critical strain can be determined by the stress-strain curve. However, both the calculation of the critical strain and the subsection processing of stress-strain curve are very complicated, so it is necessary to look for a simple method.

The stress-strain curve is an external and comprehensive reflection of the microstructural evolution and deformation mechanisms (Ref 12). It can be used to find the material constants of a constitutive model describing the laws of WH, DRV and DRX, besides the critical strain of the onset of DRX. This set of material constants would be unique if the number of different experimental tests is not less than the constants to be determined in the constitutive model. With this set of constants, we are able not only to determine the constitutive equation of the investigated steel, but also to explore quantitatively the materials science problems of WH, DRV and DRX.

The alloy studied is a low carbon bainitic steel with moderate strength, superior plasticity and good weldability. Previous investigations give a profound attention on the effect of composition and thermodynamic parameters on microstructure and mechanical properties (Ref 13-15). In this paper, a constitutive model which can reflect the deformation mechanisms of the investigated steel has been established; the critical strain and the material constants in the model have been optimized by an inverse analysis of the experimental stress-strain curve, thereby gaining the constitutive equation and the materials models of WH, DRV and DRX for this steel. At the

Lixin Li and Shengde Hu, The State Key Laboratory of Refractories and Metallurgy, Wuhan 430081, China; and Wuhan University of Science and Technology, Wuhan 430081, China; Ben Ye and Hanqing Liao, Wuhan University of Science and Technology, Wuhan 430081, China; and Sheng Liu, Key Laboratory for Ferrous Metallurgy and Resources Utilization of Ministry of Education, Wuhan 430081, China; and Wuhan University of Science and Technology, Wuhan 430081, China. Contact e-mail: linovo@126.com.

same time, the constitutive equation, the material models, and the methods of obtaining the constitutive equation and material constants have been verified by the experimental data under different deformation states.

## 2. Model Establishment

According to the linear theory of WH (Ref 16), the accumulation rate of the dislocation density is as follows:

$$\frac{\partial \rho^+}{\partial \varepsilon} = U\sqrt{\rho} \quad (\text{Eq 1})$$

where  $U = U_0 \exp(Q_u/RT)$ ;  $U_0$  is a material constant,  $\text{m}^{-1}$ ;  $Q_u$  is the activation energy of WH, J/mol;  $R$  is the gas constant, J/(mol K);  $T$  is the temperature, K;  $\rho$  is the dislocation density; and  $\varepsilon$  is the strain.

Suppose that the annihilation rate of dislocation density is a first-order reaction in DRV (Ref 17), then:

$$\frac{\partial \rho^-}{\partial \varepsilon} = -V\rho \quad (\text{Eq 2})$$

where  $V = V_0 d^{-p} \dot{\varepsilon}^{-q} \exp(Q_v/RT)$ ;  $V_0$  and  $p$  are material constants;  $d$  is the grain diameter of austenite,  $\mu\text{m}$ ;  $\dot{\varepsilon}$  is the strain rate,  $\text{s}^{-1}$ ;  $Q_v$  is the activation energy of DRV, J/mol; and  $q$  can be expressed by

$$q = c_1 + c_2 T \quad (\text{Eq 3})$$

where  $c_1$  and  $c_2$  are material constants (Ref 18).

If WH and DRV occur simultaneously, and they are independent of each other, then the variation of dislocation density takes a form of  $d\rho = (U\sqrt{\rho} - V\rho)d\varepsilon$  (Ref 19, 20), and the dislocation density  $\rho$  can be obtained in the form:

$$\sqrt{\rho} = \left[ \frac{U}{V} + \left( \sqrt{\rho_0} - \frac{U}{V} \right) \exp\left(-\frac{V}{2}\varepsilon\right) \right] \quad (\text{Eq 4})$$

where  $\rho_0$  is the initial dislocation density, which is assumed to be  $10^{12} \text{m}^{-2}$  (Ref 4).

For a coarse-grain, single-phase material, the relationship between flow stress and dislocation density can be expressed as follows (Ref 21, 22):

$$\sigma = c\mu b\sqrt{\rho} \quad (\text{Eq 5})$$

where  $c$  is a material constant;  $b$  is the magnitude of Burgers vector of dislocations, in the present work,  $b = 2.6 \times 10^{-10} \text{m}$  (Ref 4); and the temperature-dependent shear modulus can be expressed by

$$\mu = c_3 - \frac{c_4}{\exp(c_5/T) - 1} \quad (\text{Eq 6})$$

where  $c_3$ ,  $c_4$  and  $c_5$  are material constants (Ref 23, 24).

Substituting Eq 4 into 5 yields the flow stress of DRV

$$\sigma_{\text{DRV}} = \sigma_{\text{ss}} + (\sigma_0 - \sigma_{\text{ss}}) \exp\left(-\frac{V}{2}\varepsilon\right) \quad (\text{Eq 7})$$

where  $\sigma_0 = c\mu b\sqrt{\rho_0}$  is the initial stress, MPa;  $\sigma_{\text{ss}} = c\mu bU/V$  is the steady flow stress.

The combined effects of forming temperature and strain rate on deformation behavior of an alloy can be characterized by a temperature-compensated strain rate factor:

$$Z = \dot{\varepsilon} \exp(Q/RT) \quad (\text{Eq 8})$$

where  $Q$  is the deformation activation energy of alloy. The peak stress can be described as  $\sigma_p = BZ^D$  (Ref 11), where  $B$  and  $D$  are material constants. Similarly, the stress of complete DRX can be written as

$$\sigma_{\text{sx}} = AZ^m \quad (\text{Eq 9})$$

where  $A$  and  $m$  are material constants (Ref 22).

The volume fraction of DRX can be expressed by  $X_{\text{DRX}} = 1 - \exp[-k((\varepsilon - \varepsilon_c)/\varepsilon_p)^n]$  (Ref 10), where  $\varepsilon_p$  and  $\varepsilon_c$  are the peak and critical strain, respectively,  $k$  and  $n$  are material constants. Because  $\varepsilon_c = \gamma\varepsilon_p$  (Ref 25), so

$$X_{\text{DRX}} = 1 - \exp[-k(\varepsilon/\varepsilon_p - \gamma)^n] \quad (\text{Eq 10})$$

where  $\gamma$  is a material constant.

According to the law of mixtures (Ref 26), the flow stress of incomplete DRX can be expressed by

$$\sigma_{\text{DRX}} = (1 - X_{\text{DRX}})\sigma_{\text{DRV}} + X_{\text{DRX}}\sigma_{\text{sx}} \quad (\text{Eq 11})$$

Because  $X_{\text{DRX}} = 0$  in the stage of WH and DRV, so the flow stress during the process of deformation can be written as

$$\sigma = (1 - X_{\text{DRX}})\sigma_{\text{DRV}} + X_{\text{DRX}}\sigma_{\text{sx}} \quad (\text{Eq 12})$$

where  $\sigma_{\text{DRV}}$ ,  $\sigma_{\text{sx}}$ , and  $X_{\text{DRX}}$  can be determined by Eq 7, 9, and 10, respectively.

## 3. Experiment Procedures

### 3.1 Materials

The alloy studied is a Mn-Mo-B series bainite steel, its chemical compositions (wt.%) are as follows: 0.053C-0.310Si-1.567Mn-0.014P-0.005S-0.246Mo-0.014Ti-0.236Ni-0.0012B. The steel was in the form of a 30 mm × 300 mm × 450 mm plate which had been hot-rolled. Cylindrical specimens with a height of 15 mm and a diameter of 10 mm were machined from the plate. The axis of the specimen is selected in the direction of the plate thickness.

### 3.2 Method

Hot compression tests were conducted on a Gleeble-1500 thermo-mechanical simulator. Four different temperatures (1173, 1273, 1373, 1473 K) and four different strain rates (0.01, 0.1, 1, 10  $\text{s}^{-1}$ ) were used in hot compression tests. In order to minimize friction and try to keep the cylindrical shape of specimens unchanged during tests, graphite powder was put in the two grooves of a diameter of 6 mm and a height of 0.2 mm specially made on both ends of each specimen.

Specimens were first heated to 1473 K at a rate of 10 K/s, homogenized at that temperature for 5 min, and cooled to the deformation temperature at a rate of 3 K/s by cooling gas of He, then held isothermally for 2 min to eliminate the thermal gradient before deformation, and finally compressed to  $\varepsilon = \ln(H/h) = 0.7$  (Ref 11, 27).

After isothermal compression, specimens were immediately water-quenched to preserve the high-temperature microstructure. Selected deformed specimens were axially sectioned and prepared for metallographic examination using standard

techniques. All microstructures were observed by optical microscopy of Axiovert 25.

### 3.3 Results

The true stress-true strain data were recorded automatically by the testing system in the isothermal compression process. The experimental results of a strain rate of  $0.1 \text{ s}^{-1}$  and a temperature of 1373 K are illustrated in Fig. 1(a) and (b), respectively. The microstructure of a specimen deformed at 1373 K and  $0.1 \text{ s}^{-1}$  is shown in Fig. 1(c).

It can be found that there are three types of stress-strain curves: The first is characterized by the increase in flow stress with strain, which is demonstrated by the curve marked  $10 \text{ s}^{-1}$  shown in Fig. 1(b); the second is characterized by a saturation stress with increasing strain, which is displayed in the curve marked 1173 K shown in Fig. 1(a); and the last is composed of three stages: WH, softening and steady stage. In WH stage, the softening effect of DRV is too weak to balance the hardening effect of the continuous increase in dislocation, resulting in that the flow stress increases with the increase in strain. In the softening stage, the DRX occurs when the dislocation density reaches a critical value. The DRX will cause the annihilation of dislocations, and consequently, the flow stress will decrease. In the steady stage, the flow stress keeps a constant nearly due to the balance between the WH and dynamic softening (Ref 4).

## 4. Analysis

### 4.1 Data Treatment

There will be 16 constants to be determined for establishing a stress-strain relationship of the steel investigated; they are material constants of  $c, c_1, c_2, c_3, c_4, c_5, U_0, Q_u, V_0 d^{-P}, Q_s, k, n, \gamma, Q_s, A$  and  $m$ . Let the stress measured by experiment and the one calculated from Eq 12 at a strain of  $\varepsilon_i$  be  $\sigma_{mi}$  and  $\sigma_{ci}$ , respectively, the material constants can then be obtained by minimizing the value of function  $y = \sum_{i=1}^{n_i} (1 - \sigma_{ci}/\sigma_{mi})^2$  (where  $n_i$  is the group number of strain-stress measured experimentally). This optimizing procedure is to ensure that the stress-strain curves calculated from the material constants are the closest to those measured experimentally.

The coordinate rotation method is a common optimization technique. The computation is carried out along each coordi-

nate direction alternately, in which only the value of the optimized coordinate is changed, whereas other variables remain unchanged. The optimal values obtained by the coordinate rotation method with a convergence accuracy of 0.5% for each optimization parameter are shown in Table 1.

The relationship between the shear modulus of steel and temperature can be determined by substituting the optimal material constants into Eq 6:

$$\mu = 8881.92 - \frac{924.01}{\exp[165.62/T] - 1} \quad (\text{Eq 13})$$

Parameter  $q$  can be determined by equation:

$$q = 0.05066 + 6.87 \times 10^{-5} T \quad (\text{Eq 14})$$

The activation energy of WH  $Q_u = 2.6177 \times 10^4 \text{ J/mol}$ , and

$$U = 7.1104 \times 10^8 \exp\left(-\frac{26,177.11}{RT}\right) \quad (\text{Eq 15})$$

The activation energy of DRV  $Q_v = 3.7214 \times 10^4 \text{ J/mol}$ , so

$$V = 1080.66 \dot{\varepsilon}^{-0.05066 - 6.87 \times 10^{-5} T} \exp\left(-\frac{37,214.84}{RT}\right) \quad (\text{Eq 16})$$

The volume fractions of DRX

$$X_{\text{DRX}} = 1 - \exp\left[-0.593085(\varepsilon/\varepsilon_p - 0.886463)^{1.833593}\right] \quad (\text{Eq 17})$$

The activation energy of deformation  $Q = 436,587.88 \text{ J/mol}$ . The flow stress of complete DRX can be expressed by

$$\sigma_{sx} = 0.0868332Z^{0.169886} \quad (\text{Eq 18})$$

Besides, according to (Ref 18), the volume fractions of DRV

$$X_{\text{DRV}} = 1 - \exp\left[-540.33 \dot{\varepsilon}^{-0.05066 - 6.87 \times 10^{-5} T} \exp(-37,214.84/RT)\varepsilon\right] \quad (\text{Eq 19})$$

### 4.2 Experimental Verification

A comparison between the experimental and calculated stress-strain curves was carried out in a wide range of strain, strain rate, and temperature to verify the accuracy of the constitutive equation. The results show a good agreement of the calculated and experimental curves under entire experimental

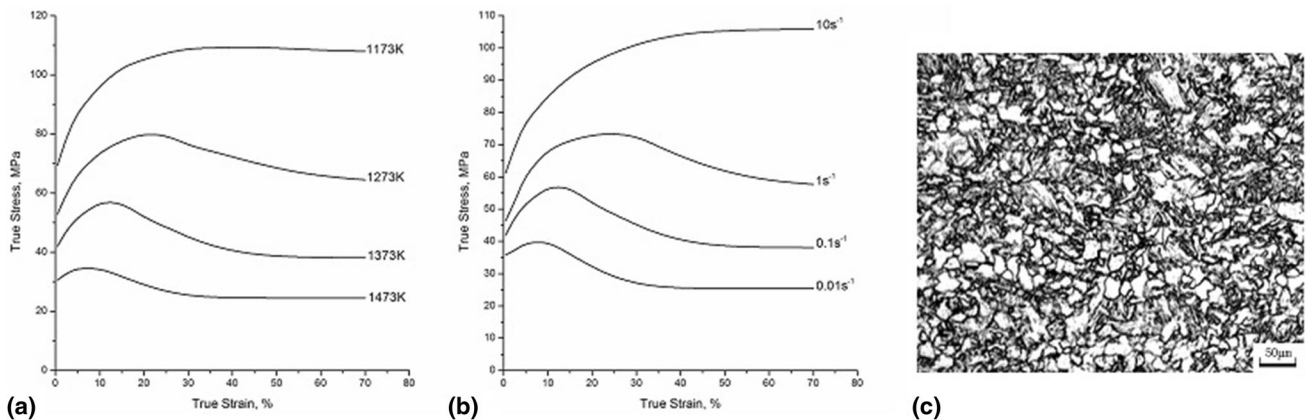


Fig. 1 Experimental stress-strain curves and microstructure of a specimen deformed at 1373 K and  $0.1 \text{ s}^{-1}$

conditions. As an example, the results of a temperature of 1273 K and a strain rate of  $1 \text{ s}^{-1}$  are shown in Fig. 2(a) and (b), respectively.

Another comparison between the experimental and calculated values of flow stress is shown in Fig. 2(c). The slope of the regression line is 1.00506, showing that most of the data points lie fairly close to the best regression line. The correlation coefficient is 0.994862, indicating that a good correlation between the experimental and calculated data was achieved.

It is also shown that the relative errors of flow stress are mostly  $<3\%$  except when the strain is  $<0.026$ , and the average absolute relative error is 3.56%. Obviously, the constitutive equation with its higher precision can be used to calculate the energy consumption and to analyze the deformation process of the steel. Average absolute relative error can be used as an unbiased statistical parameter for evaluating the deviation from the predicted flow stress; therefore, the constitutive equation based on dislocation theory, WH and DRV theory and softening mechanism of DRX can well describe the high-temperature deformation behavior of the investigated steel.

## 5. Discussion

### 5.1 The Material Constant

A comparison of material constants between literature (Ref 18) and this paper is shown in Table 2. It indicates that the values obtained by two different methods are similar.

### 5.2 The Flow Stress of Complete DRX

A comparison of flow stresses of complete DRX between the experimental and calculated by Eq 18 is shown in Fig. 3(a).

The correlation coefficient of 0.977328 indicates that the calculated values agree well with those measured, demonstrating that the material constants determined by the stress-strain curves and the constitutive model can capture the underlying materials science of high-temperature deformation.

### 5.3 The Critical Stress of DRX

The ratio of critical strain to peak strain equals to 0.886463 according to Eq 17, which is located between 0.6 and 0.9 as (Ref 28) indicated. The critical stress  $\sigma_c$  of DRX can be calculated by applying this relationship to the stress-strain data measured in different deformation parameters, or by using the criterion of  $\frac{\partial}{\partial \sigma} \left( -\frac{\partial \theta}{\partial \sigma} \right) = 0$ . A comparison of the critical stresses determined by the two methods is shown in Fig. 3(b). Clearly, both results are in good agreement.

The relation between  $\sigma_c$  and the peak stress  $\sigma_p$  is  $\sigma_c = (0.997658 \pm 0.0008502)\sigma_p$ , meaning the critical stress is about 0.25% smaller than the peak one. The linear regression of the peak stresses measured and the values of  $Z$  determined by Eq 8 results in the material constants  $B = 0.434786$  and  $D = 0.13326$ , meaning  $\sigma_p = 0.434786Z^{0.13326}$ . Similarly, the critical stress can be expressed as  $\sigma_c = 0.436158Z^{0.1331}$ , so  $\sigma_c/\sigma_p = 1.003155Z^{-0.00016}$ , indicating that the smaller the Zener-Hollomon parameter is, the smaller the difference between  $\sigma_c$  and  $\sigma_p$ .

### 5.4 Kinetics of DRV and DRX

The kinetics of DRV can be determined by Eq 19. The variations in the volume fraction of DRV with strain at deformation temperature of 1173 K are shown in Fig. 4(a). Similarly, the kinetics of DRX can be calculated by Eq 17. The variations in the volume fraction of DRX with strain at a strain

**Table 1** Optimal values

Symbol (Equation no.)	$U_0$ (Eq 1)	$Q_u$ (Eq 1)	$V_0 d^{-p}$ (Eq 2)	$Q_v$ (Eq 2)	$c_1$ (Eq 3)	$c_2$ (Eq 3)	$c$ (Eq 5)	$c_3$ (Eq 6)
Optimal value	7.1104e+8	26,177.11	1080.66	37,214.84	0.05066	6.87e-5	99.6196	8881.92
Symbol (Equation no.)	$c_4$ (Eq 6)	$c_5$ (Eq 6)	$Q$ (Eq 8)	$A$ (Eq 9)	$m$ (Eq 9)	$k$ (Eq 10)	$n$ (Eq 10)	$\gamma$ (Eq 10)
Optimal value	924.01	165.62	436,587.88	0.0868332	0.169886	0.593085	1.833593	0.886463

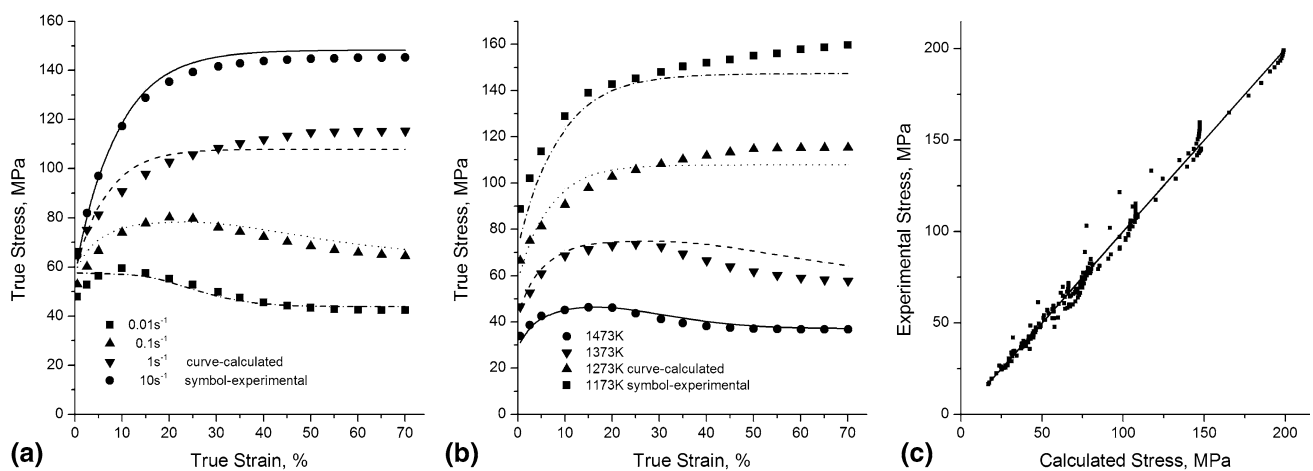


**Fig. 2** Comparison between calculated and experimental stresses

**Table 2 Comparison of material constants**

Material parameters	$c$	$c_1$	$c_2$	$c_3$	$c_4$	$c_5$	$U_0$	$Q_u$	$V_0 d^{-p}$	$Q_v$	$Q$
Value in (Ref 18)	104.1544	0.05169	7.05e-5	9282.97	942.12	162.02	7.1205e+8	27,112.52	1030.13	36,764.20	422,478
Value in this paper	99.6196	0.05066	6.87e-5	8881.92	924.01	165.62	7.1104e+8	26,177.11	1080.66	37,214.84	436,588
Relative error/%	-4.354	-1.993	-2.553	-4.320	-1.922	2.222	-0.142	-3.450	4.905	1.226	3.340

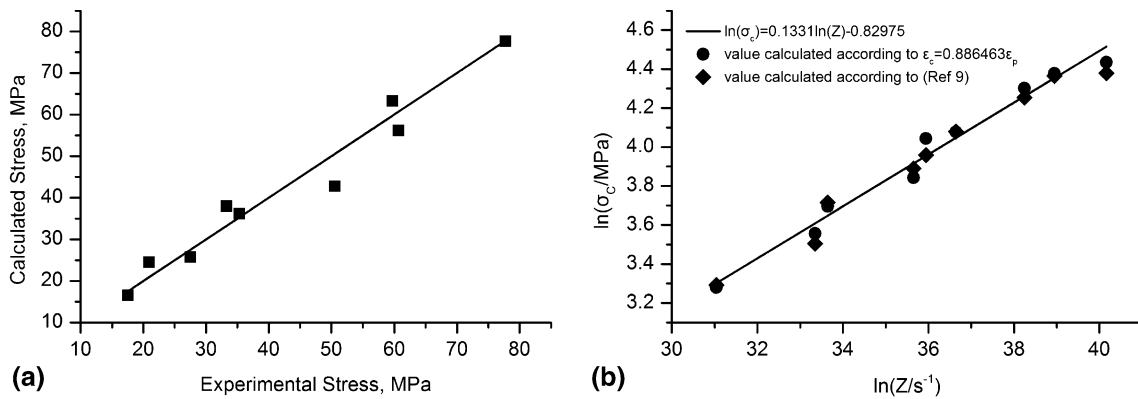


**Fig. 3** Comparison between the calculated and experimental stresses of complete DRX (a) and initiation of DRX (b)

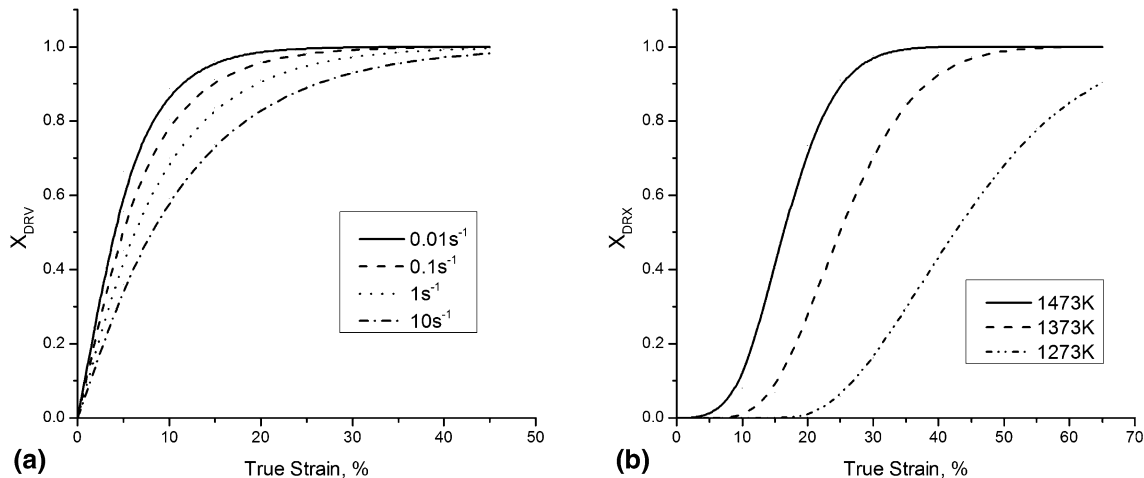


**Fig. 4** Variations of  $X_{DRV}$  and  $X_{DRX}$  with strain under different deformation parameters

rate of  $0.1 \text{ s}^{-1}$  are shown in Fig. 4(b). As expected, the volume fractions of DRV or DRX increase with the increase in strain. The smaller the strain rate is, the smaller the strain of complete DRV. The higher the deforming temperature is, the faster the process of DRX.

## 6. Conclusion

A constitutive model during high-temperature deformation can be established based on dislocation theory, work hardening and dynamic recovery theory, and softening mechanisms of dynamic recrystallization. An inverse analysis of the stress-strain curve measured experimentally has been proposed to determine the model constants for the relevant materials science and to establish the constitutive equation. Predictions of materials science models and the constitutive equation are in

good agreement with the test results of stress-strain curves for a bainite steel. This agreement confirms that the constitutive model and the inverse analysis method are effective to determine the material constants and the constitutive equation from the measured stress-strain data. The analysis method can be extended to other coarse-grain, single-phase alloys.

## References

1. Z. Akbari, H. Mirzadeh, and J.-M. Cabrera, A Simple Constitutive Model for Predicting Flow Stress of Medium Carbon Microalloyed Steel During Hot Deformation, *Mater. Des.*, 2015, **77**, p 126–131
2. E.S. Puchi-Cabrera, J.D. Guerin, M. Dubar, M.H. Staia, J. Lesage, and D. Chicot, Constitutive Description of Fe-Mn23-C0.6 Steel Deformed Under Hot-Working Conditions, *Int. J. Mech. Sci.*, 2015, **99**, p 143–153
3. D. Feng, X.M. Zhang, S.D. Liu, and Y.L. Deng, Constitutive Equation and Hot Deformation Behavior of Homogenized Al-7.68Zn-2.12Mg-1.98Cu-

- 0.12Zr Alloy During Compression at Elevated Temperature, *Mater. Sci. Eng. A*, 2014, **608**, p 63–72
4. T. Yan, E. Yu, and Y. Zhao, Constitutive Modeling for Flow Stress of 55SiMnMo Bainite Steel at Hot Working Conditions, *Mater. Des.*, 2013, **50**, p 574–580
  5. S.V. Mehtonen, L.P. Karjalainen, and D.A. Porter, Modeling of the High Temperature Flow Behavior of Stabilized 12-27 wt% Cr Ferritic Stainless Steels, *Mater. Sci. Eng. A*, 2014, **607**, p 44–52
  6. Y.G. Liu, M.Q. Li, and J. Luo, The Modelling of Dynamic Recrystallization in the Isothermal Compression of 300 M Steel, *Mater. Sci. Eng. A*, 2013, **574**, p 1–8
  7. B. Wu, M.Q. Li, and D.W. Ma, The Flow Behavior and Constitutive Equations in Isothermal Compression of 7050 Aluminum Alloy, *Mater. Sci. Eng. A*, 2012, **542**, p 79–87
  8. I. Mejia, G. Altamirano, A. Bedolla-Jacuinde, and J.M. Cabrera, Modeling of the Hot Flow Behavior of Advanced Ultra-High Strength Steels (A-UHSS) Microalloyed with Boron, *Mater. Sci. Eng. A*, 2014, **604**, p 116–125
  9. E.I. Poliakt and J.J. Jonas, A One-Parameter Approach to Determining the Critical Conditions for the Initiation of Dynamic Recrystallization, *Acta Mater.*, 1996, **44**, p 127–136
  10. M. Wang, Y. Li, W. Wang, J. Zhou, and A. Chiba, Quantitative Analysis of Work Hardening and Dynamic Softening Behavior of low Carbon Alloy Steel Based on the Flow Stress, *Mater. Des.*, 2013, **45**, p 384–392
  11. X.-M. Chen, Y.C. Lin, D.-X. Wen, J.-L. Zhang, and M. He, Dynamic Recrystallization Behavior of a Typical Nickel-Based Superalloy During Hot Deformation, *Mater. Des.*, 2014, **57**, p 568–577
  12. M.A. Mostafaei and M. Kazeminezhad, A Novel Approach to Find the Kinetics of Dynamic Recovery Based on Hot Flow Curves, *Mater. Sci. Eng. A*, 2012, **544**, p 88–91
  13. W.F. Cui, S.X. Zhang, Y. Jiang, J. Dong, and C.M. Liu, Mechanical Properties and Hot-Rolled Micro-Structures of a Low Carbon Bainitic Steel with Cu-P Alloying, *Mater. Sci. Eng. A*, 2011, **528**, p 6401–6406
  14. H.K. Sung, D.H. Lee, S.Y. Shin, S. Lee, J.Y. Yoo, and Y. Hwang, Effect of Finish Cooling Temperature on Microstructure and Mechanical Properties of High-Strength Bainitic Steels Containing Cr, Mo, and B, *Mater. Sci. Eng. A*, 2015, **624**, p 14–22
  15. X. Kong, L. Lan, Z. Hu, B. Li, and T. Sui, Optimization of Mechanical Properties of High Strength Bainitic Steel Using Thermo-Mechanical Control and Accelerated Cooling Process, *J. Mater. Process. Technol.*, 2015, **217**, p 202–210
  16. R. Sandstrom, On Recovery of Dislocations in Subgrains and Subgrain Coalescence, *Acta Metall.*, 1977, **25**, p 897–904
  17. E.I. Galindo-Nava, J. Sietsma, and P.E.J. Rivera-Diaz-del-Castillo, Dislocation Annihilation in Plastic Deformation: II. Kocks-Mecking Analysis, *Acta Mater.*, 2012, **60**, p 2615–2624
  18. L. Li, B. Ye, S. Liu, S. Hu, and B. Li, Inverse Analysis of the Stress-Strain Curve to Determine the Materials Models of Work Hardening and Dynamic Recovery, *Mater. Sci. Eng. A*, 2015, **636**, p 243–248
  19. E.I. Galindo-Nava and P.E.J. Rivera-Diaz-del-Castillo, Modelling Plastic Deformation in BCC metals: Dynamic Recovery and Cell Formation Effects, *Mater. Sci. Eng. A*, 2012, **558**, p 641–648
  20. D.-W. Suh, J.-Y. Cho, K.H. Oh, and H.-C. Lee, Evaluation of Dislocation Density from the Flow Curves of Hot Deformed Austenite, *ISIJ Int.*, 2002, **42**, p 564–569
  21. U.F. Kocks and H. Mecking, Physics and Phenomenology of Strain Hardening: the FCC Case, *Prog. Mater. Sci.*, 2003, **48**, p 171–273
  22. X.G. Fan, H. Yang, Z.C. Sun, and D.W. Zhang, Quantitative Analysis of Dynamic Recrystallization Behavior Using a Grain Boundary Evolution Based Kinetic Model, *Mater. Sci. Eng. A*, 2010, **527**, p 5368–5377
  23. C. Wu, H. Yang, and H.W. LI, Simulated and Experimental Investigation on Discontinuous Dynamic Recrystallization of a Near- $\alpha$ TA15 Titanium Alloy During Isothermal Hot Compression in  $\beta$ Single-Phase Field, *Trans. Nonferrous Met. Soc. China*, 2014, **24**, p 1819–1829
  24. R. Liu, M. Salahshoor, S.N. Melkote, and T. Marusich, A Unified Internal State Variable Material Model for Inelastic Deformation and Microstructure Evolution in SS304, *Mater. Sci. Eng. A*, 2014, **594**, p 352–363
  25. X. Liang, J.R. McDermid, O. Bouaziz, X. Wang, J.D. Embury, and H.S. Zurob, Microstructural Evolution and Strain Hardening of Fe-24Mn and Fe-30Mn Alloys During Tensile Deformation, *Acta Mater.*, 2009, **57**, p 3978–3988
  26. L. Delannay, P. Jacques, and T. Pardoen, Modelling of the Plastic Flow of Trip-Aided Multiphase Steel Based on an Incremental Mean-Field Approach, *Int. J. Solids Struct.*, 2008, **45**, p 1825–1843
  27. J. Zhang, H. Di, X. Wang, Y. Cao, J. Zhang, and T. Ma, Constitutive Analysis of the Hot Deformation Behavior of Fe-23Mn-2Al-0.2C Twinning Induced Plasticity Steel in Consideration of Strain, *Mater. Des.*, 2013, **44**, p 354–364
  28. L.P. Karjalainen, T.M. Maccagno, and J.J. Jonas, Softening and Flow Stress Behaviour During Hot Rolling Simulation of Nb Microalloyed Steels, *ISIJ Int.*, 1995, **35**, p 1523–1531